

Development of GaN/AlGaN UVAPDs for Ultraviolet Sensor Applications

Ashok K. Sood, John W. Zeller, Roger E. Welser and Yash R. Puri

Magnolia Optical Technologies Inc., 52-B Cummings Park, Woburn, MA 01801

Russell D. Dupuis, Mi-Hee Ji, Jeomoh Kim and Theeradetch Detchprohm

School of Electrical Engineering, Georgia Institute of Technology, Atlanta, GA 30332

Jay Lewis

DARPA/MTO, 675 North Randolph Street, Arlington, VA 22203

Nibir K. Dhar

*Night Vision & Electronic Sensors Directorate, 10221 Burbeck Road Fort Belvoir,
VA 22060*

Roy L. Peters

AQD, US Department of Interior, Sierra Vista, Arizona 85636

ABSTRACT

High-resolution imaging in ultraviolet (UV) bands has many applications in defense and commercial systems. The shortest wavelength is desired for increased spatial resolution, which allows for small pixels and large formats. In past work, UV avalanche photodiodes (APDs) have been reported as discrete devices demonstrating gain. The next frontier is to develop UVAPD arrays with high gain to demonstrate high-resolution imaging.

We will discuss a model that can predict sensor performance in the UV band using APDs with various gain and other parameters for a desired UV band of interest. Signal-to-noise ratios (SNRs) can be modeled from illuminated targets at various distances with high resolution under standard atmospheric conditions in the UV band and the solar-blind region using detector arrays with unity gain and with high-gain APDs.

We will present recent data on the GaN-based APDs for their gain, detector response, dark current noise, and 1/f noise. We will discuss various approaches and device designs that are being evaluated for developing APDs in wide-bandgap semiconductors. The paper will also discuss the state of the art in UVAPDs and the future directions for small unit cell size and gain in the APDs.

APPLICATIONS OF UV IMAGING TECHNOLOGY

Imagery for identification of targets at various distances uses visible cameras, image intensifiers, shortwave-infrared (SWIR) cameras, and long wave-IR (LWIR) uncooled cameras. Each has distinct advantages and disadvantages, and each is useful under specific sets of conditions such as light level, thermal conditions, and level of atmospheric obscuration. The shortest wavelength is desired for spatial resolution, which allows for small pixels and large formats [1-5].

If an adequate light level is present, visible cameras can provide high resolution, but for long-range identification even under moonlit and starlit illuminations, long integration times and large optics are required, as dust, smoke and fog easily defeat a single visible camera. Image intensifiers and SWIR cameras are useful in many conditions, as the SWIR penetrates fog easily but requires fairly clear night skies for the upper atmospheric airglow light source, and image intensifiers require a certain level of celestial (starlight, moonlight) or light pollution irradiance. Both the SWIR cameras and image intensifiers are limited by the diffraction resolution of the near-IR (NIR) to SWIR wavelengths [5].

For optimal resolution, the visible or ultraviolet spectrum is preferable; however, active (laser) illumination is required for long-range night imaging. Covert UV illumination is preferred over the visible, and the atmosphere transmits fairly well at the longer UV wavelengths. The covert active system for high-resolution identification modeled in this paper consists of a UV laser source and a silicon CCD, AlGaIn, or AlGaIn APD focal plane array (FPA) with pixels as small as 4 microns that are spectrally tuned for the solar-blind region of the UV spectrum. The solar-blind region is optimal, as virtually all of the solar radiation is absorbed at the higher altitudes, leaving a pitch-dark terrain even in bright daylight; yet for sea-level pathlengths of 1 km and shorter, the UV atmospheric transmittance is still acceptable.

This combination is ideal for exploitation by a UV illuminator and UV FPA sensor. Current UV lasers can provide either continuous or pulsed energy at levels detectable by solar-blind UV detectors under relatively small optics and at 30 Hz frame rates, providing real-time high-resolution (on the order of 1 cm at 1 km) imagery. At these illumination levels and target ranges, standard PN, PIN and APD UV detectors and silicon CCDs can be used for target identification. The model has been developed and used to include the combined effects of detector and electronics, atmospheric transmittance and UV background radiance, target size, range and reflectance, and UV laser attributes to simulate and predict both CW and pulsed laser imaging performance and to assist in the design of this prototype system [5].

MODEL DEVELOPMENT FOR PASSIVE AND ACTIVE UV SYSTEMS DESIGN

The general equations for SNR prediction for laser illumination and APD are derived

$$SNR = \frac{Ge_{Lret}}{[F^2G^2(e_{Lret} + e_{bk} + e_{dk}) + (\tilde{e}_{n,amp})^2]^{1/2}} \quad (1)$$

where G is the APD gain, F is the excess noise, the noise electron terms are the laser return shot noise, the scene noise, the dark current noise and the amp noise.

Two special and frequently-occurring cases are (2) for the laser power noise-limited case and (3) for the amp noise-limited case:

$$SNR = \frac{[e_{Lret}]^{1/2}}{F} \quad (2)$$

$$SNR = \frac{Ge_{Lret}}{(\tilde{e}_{n,amp})} \quad (3)$$

The laser return in electrons for cw assuming lambertian reflection is:

$$e_{Lret,ti} = [t_i \eta \tau_o] [P_{Lcw} \frac{\lambda}{hc}] \tau_a \frac{\Omega_{pix}}{\Omega_L} \rho_{tar} \tau_a^2 \frac{A_o}{\pi R^2} = [t_i \eta \tau_o] [P_{Lcw} \frac{\lambda}{hc}] \tau_a \frac{4A_{pix}}{\pi \theta_{div}^2 f^2} \rho_{tar} \tau_a^2 \frac{A_o}{\pi R^2} \quad (4)$$

Or when separated into detector/optics, atmosphere, laser and target attributes:

$$e_{Lret,ti} = [t_i \eta \tau_o \frac{A_{pix} A_o}{\pi f^2}] \tau_a^2 \frac{[\Phi_{Lcw}]}{\theta_{div}^2} \frac{4\rho_{tar}}{\pi R^2} \quad (5)$$

If we allow for frame summing:

$$e_{Lret,ti+} = N_{fs} [t_i \eta \tau_o \frac{A_{pix} A_o}{\pi f^2}] \tau_a^2 \frac{[\Phi_{Lcw}]}{\theta_{div}^2} \frac{4\rho_{tar}}{\pi R^2} \quad (6)$$

For pulse laser operation and using t_{bin} which equals t_{pulse} and the number of bins per frame $N_{bins/f}$:

$$e_{Limage} = [N_{bins/f} \eta \tau_o \frac{A_{pix} A_o}{\pi f^2}] \tau_a^2 \frac{P_{Lpulse} (\lambda / hc)}{\theta_{div}^2} \frac{4\rho_{tar}}{\pi R^2} \quad (7)$$

SPECTRAL BANDS		LASER		SCENE / TARGET TIMING					
lam hi	0.267 um	lambda	0.266 um	t transit	3.33E-06 sec	lin overfill			
lam lo	0.265 um	P laser cont	0.10 w		3333 nsec		1.25		
lam mid	0.266 um	Pd laser cont	3.18E-06 W/cm2		3.33 usec	FPA FOV (ft)	5.25		
del lam	0.002 um	Ph laser cont	1.34E+17 pho/sec	N pulses/fr	9999 max poss				
DETECTOR / FPA		Ph laser cont frame	4.46E+15 pho/frame						
format	256	E laser pulse	5.00E-06 pulse/pulse	j/frame					
dpix	5 um	Ph laser pulse	6.69E+12 pho/pulse		3.33E-03				
	2.50E-07 cm2	Ph laser bin	6.69E+12 pho/bin	watts					
ti cont	33.33 msec	div full	4 mrad	0.100					
t bin	20 nsec	t pulse	20 nsec						
t quench	3000 nsec	w pulse	6 meters						
gain	1	bin and pulse rates		det based	mission based	det/mssion min	min in kHz		
gain apd	1	sample rate (max) Hz	3.31E+05	3.00E+05	3.00E+05	300.0			
Fm noise	1	N pulses/frame	11036	9999	9999	300.0	666.6		
amp noise	5.80E+10	N bins/frame	11036	9999	9999	500.0	666.6		
tau opt	0.90	Plaser tar (cm, cm ²)	200	3.14E+04	1				
qe	0.70	diameter laser at target	6.56 ft	q factor					
eta inj	1.00	ELECTRONS AND NOISE from laser, scene, dark current and amp						647.5	
fill factor	0.75		electrons frame full int	electrons for bins in frame	electrons per bin	noise e frame full int	noise e for bins in frame	noise e per bin	
I dark	5.00E-16 a	e laser ret (s)	9713.1	647.5	9.71E-01	98.55	25.45	9.86E-01	
J dark	2.00E-09 a/cm ²	e laser ret cont	647.5	na	na	25.45	na	na	
I surface	1.00E-21 a	elect scene (b)	0	9.73E-17	1.46E-19	0.00	0.00	3.82E-10	
Rload	1.00E+06 ohm	e dark (d)	104	4.16E-02	6.24E-05	10.20	0.20	7.90E-03	
resp frame	1.57E-02	e surface	2.08E-04	8.32E-08	1.25E-10	0.01	0.00	1.12E-05	
resp bin	9.45E-09	e kT amp				10.00	0.77	7.74E-03	
	0.63					14.26	0.80		
OPTICS		MODE	signal	noise s+b+d	noise b+d	SNR s+b+d	SNR b+d	SNR s+b+d	SNR b+d
dopt	20 cm	DDLm cont	647.5	29.2	14.3	22.2	45.3	44.4	90.7
Aopt	314.16 cm2	DDLm bins sum	647.5	25.4	0.3	25.4	2267.2	50.9	4534.3
focal length	40 cm								
fnum	2.00								

Figure 1: UV Sensor Model for UV Sensor Performance

SYSTEMS PERFORMANCE METRICS FOR PASSIVE AND ACTIVE UV SYSTEMS DESIGN

To model the sensor and system performance, we have assumed the pixel size for a high-sensitivity detector of 5-20 microns for the UV-APDs. The fill factor of 70% is assumed to be typical for these small pixels. Typical quantum efficiencies have been assumed to be in the 70% range for the PIN diode and APD [1-5]. The model uses as default an amp noise of 15 electrons per frame time, a dark current of 1e-15 amps for a 5-micron pixel, or 4 nA/cm² or 200 electrons or about 14 noise electrons; scene noise is effectively zero in the solar-blind region.

In the model from the MODTRAN simulations shown in Figure 1, the daytime irradiance in the UV is insignificant in the solar-blind region. The drop-off from 0.30 microns to 0.26 microns illustrates that the requirement for a UV detector with spectral response is in the solar-blind region. Figure 2 shows the UV spectral radiance at midday and the comparative laser illumination of the target at 1 km for a 6 milliradian beam divergence for powers of 1 mW and 10 mW. The left plot in the figure shows that the transmittance improves with longer UV wavelengths for all three levels of aerosols and is sufficient for 1 km lengths in our solar-blind region.

To achieve high-resolution day-night imaging and identification of targets, the following conditions and requirements must be met. While linear detection (no APD and no laser illumination) is fine for muzzle flashes and images of nearby combatants illuminated by live fire (a millisecond event), laser illumination is required for cold targets (facial recognition, profile recognition). A continuous laser and 33

msec integrations are adequate if enough laser power is available. If not, a pulsed laser with nanosecond integrations and APD detectors are required to reduce atmosphere scatter and improve detector sensitivity.

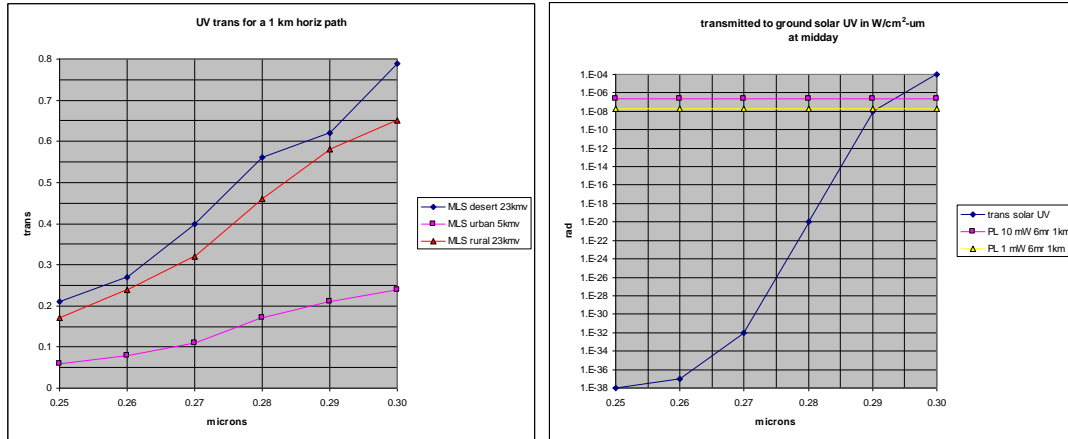


Figure 2: UV transmittance vs. wavelength for three aerosol levels (left) and UV radiance at sea level during midday and laser irradiance on the target at 1 km (6 mradian beam) from a 1mW and 10mW UV laser (right)

GaN /AlGaN UV-APD Growth

Figure 3 presents the MOCVD growth systems for GaN and AlGaN using Thomas Swan MOCVD Reactors. The GaN/ AlGaN epitaxial materials were grown by metal organic chemical vapor deposition (MOCVD) using a reactor system equipped with a Close-Coupled Showerhead (CCS) growth chamber as shown in figure 3 [6, 7].



Figure 3: MOCVD III-N Systems. Two Thomas Swan CCS 6x2 MOCVD reactors used for the development of GaN/AlGaN based UV-APDs at Georgia Institute of Technology.



Figure 4: New-generation AIXTRON CCS 3x2"; High-temperature III-Nitride 3x2" MOCVD growth chamber open for loading wafers and showing close-coupled showerhead.

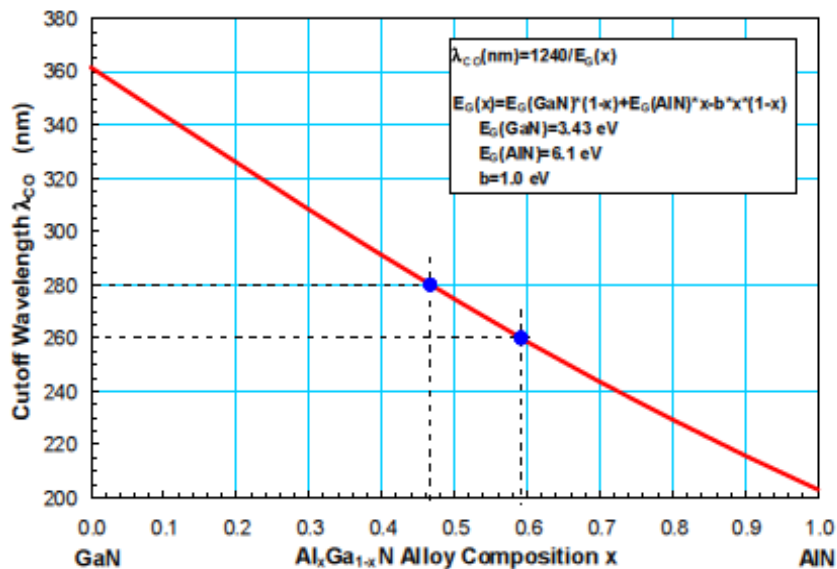


Figure 5: Relationship between alloy composition of AlGa_{1-x}N and the corresponding spectral cutoff for the UV detector arrays [3].

Figure 4 presents the High-Temperature MOCVD system by Aixtron. This new capability will allow the ability to grow high-quality GaN and AlGa_{1-x}N material with doping for GaN/AlGa_{1-x}N UV-APD applications.

Figure 5 presents the relationship between the alloy composition of Gallium and Aluminum in Al_xGa_{1-x}N that determines the cut-off wavelength of the UV

detector for *p-i-n* [3] and also for UV-APDs. Deep Ultra Violet (DUV) will require the addition of a larger composition of Aluminum in $\text{Al}_x\text{Ga}_{1-x}\text{N}$. [3].

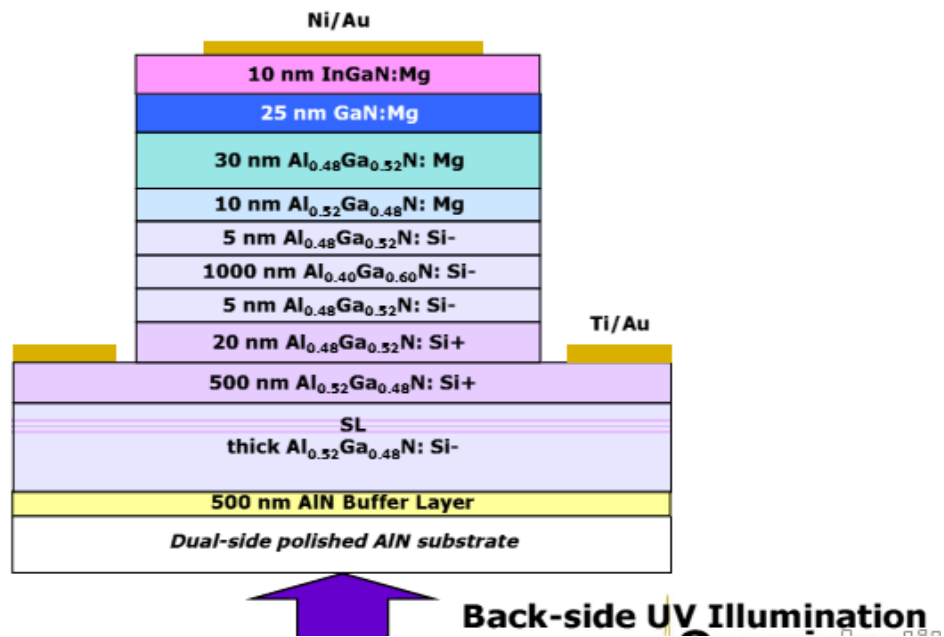


Figure 6: Device structure cross-section of prototype back-side illuminated AlGaN UV-APD.

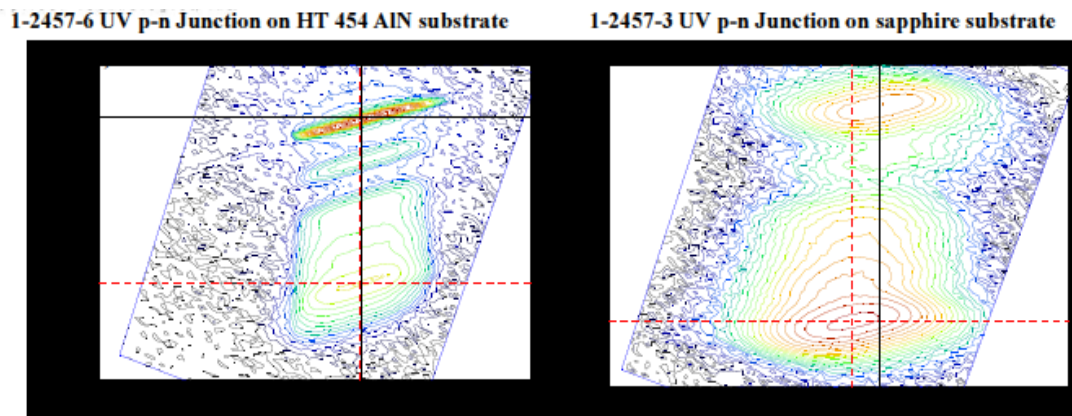


Figure 7: Reciprocal space mapping of AlGaN *p-n* junctions grown on AlN and sapphire substrates.

Figure 6 presents the device structure of a back-side-illuminated AlGaN UV-APD. The substrate in this device structure is double-side-polished AlN substrate. The use of an AlN substrate allows the UV-APD device structure to be back-side illuminated and can be integrated with silicon CMOS electronics. Figure 7 presents the reciprocal space mapping of AlGaN on the AlN substrate and sapphire substrate.

The data for the sapphire substrate shows increased strain and mosaicity compared with AlN substrate.

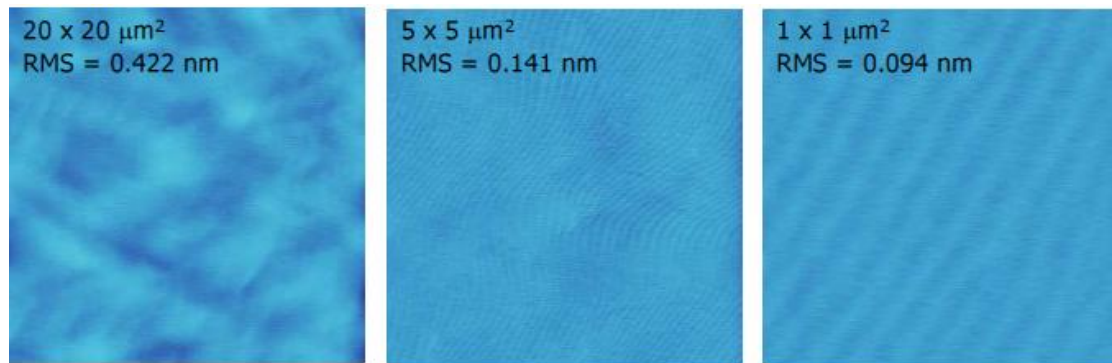


Figure 8: Microscopic surface morphology using AFM of a GaN *p-i-n* structure grown on a GaN/Sapphire template. No specific surface defects are observed.

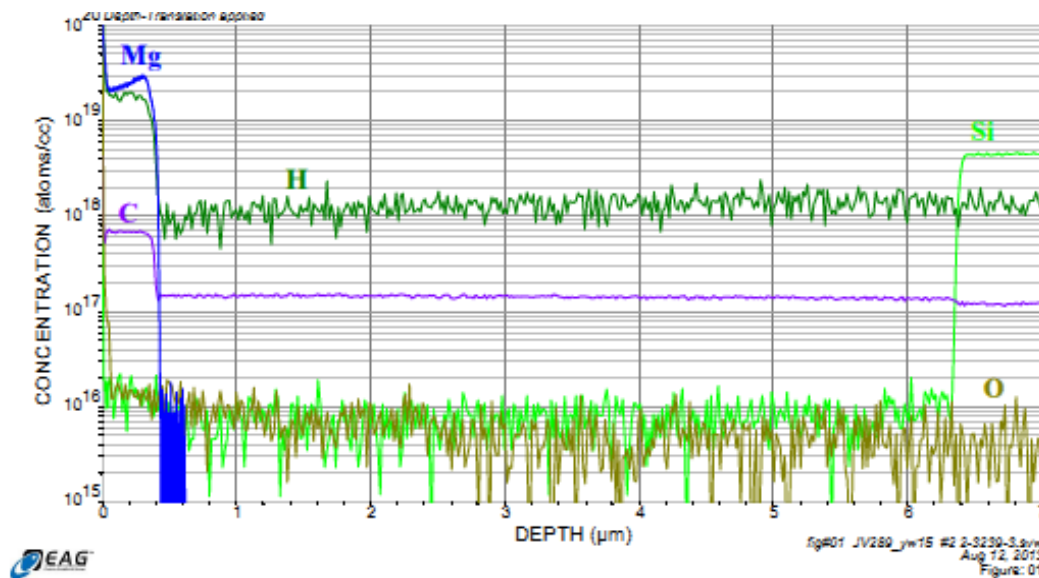


Figure 9: SIMS analysis of GaN *p-i-n* structure on GaN/Sapphire template. The data shows controlled Si and Mg doping for *n*- and *p*-type layers. The data shows low background doping concentration in *i*-GaN layer.

Figure 8 presents the microscopic surface morphology using AFM on GaN *p-i-n* structure grown on a GaN/Sapphire template. No surface defects are observed. These results are encouraging development of a low-cost, back-side-illuminated UV-APD detector array.

Figure 9 presents the SIMS analysis of the GaN *p-i-n* structure on a GaN/Sapphire template. The data show controlled Si and Mg doping for *n*- and *p*-type

layers. The data show low background doping concentration in the GaN layer. The Mg doping is being increased for better p -type conductivity.

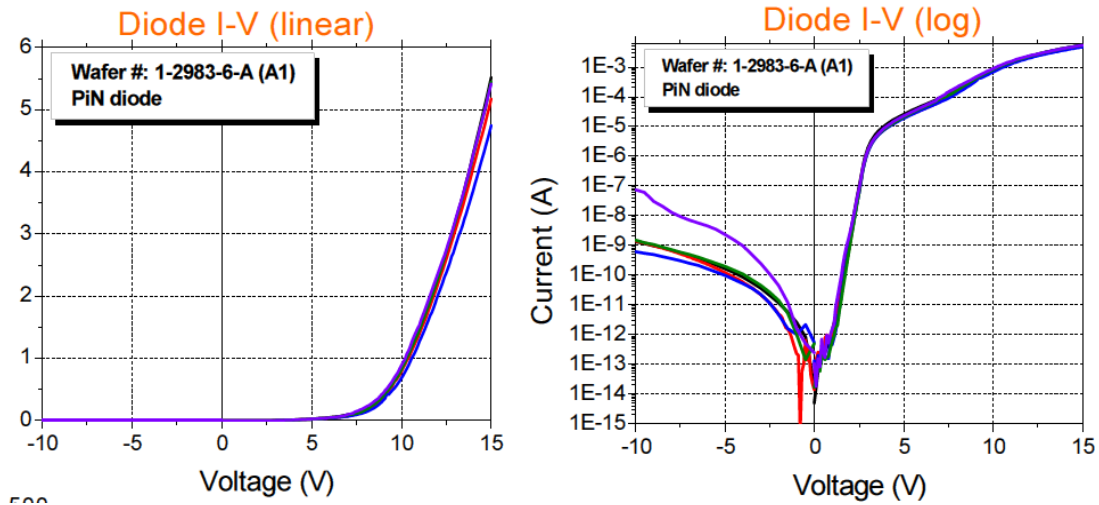


Figure 10: Current-voltage characteristics of a prototype AlGaN UV-APD unpassivated test structure. Further reduction in the dark current will be expected with surface passivation.

Figure 10 presents the current-voltage characteristics of a prototype AlGaN UVAPD designed for a spectral response of ~ 280 nm. Further reductions in the dark current will be expected with surface passivation. Efforts are underway to improve the growth and device characteristics. We believe that low-defect-density native substrates and high-quality MOCVD epitaxial growth technologies are the keys to the successful implementation of robust high-performance APDs for UV focal plane arrays.

SUMMARY

High-resolution imaging in UV bands has many applications in defense and commercial systems. We have discussed a model under development for UV imaging applications. The preliminary simulation results using MODTRAN show that high SNRs can be achieved with targets at 1 km in the solar-blind region using UV-APD arrays with low noise and high gain. With this model we can predict sensor performance in the UV band using APDs with various gain and other parameters for a desired UV band of interest. SNRs can be modeled from illuminated targets at various distances with high resolution under standard atmospheres in the UV band and the solar-blind region using detector arrays with high-gain APDs.

We have presented data on growth and characterization of GaN/ AlGaN epitaxial device structures. We have discussed various approaches and device designs that are being evaluated for developing APDs in wide-bandgap semiconductors. The

paper also discusses the future directions for small unit cell size and high gain in the APDs.

REFERENCES

1. J. P. Long, "UV detectors and focal plane array imagers based on AlGaIn p-i-n photodiodes," *Opto-Electronics Review*, Vol. 10(4), 251-260 (2002).
2. M. Crawford, "Advances in AlGaIn-based deep UV LEDs," *MRS Proceedings*, Vol. 831, Fall 2004.
3. M. B. Reine, "Solar-blind AlGaIn 256x256 p-i-n detectors and focal plane arrays," *Proc. of SPIE*, Vol. 6119 (2006).
4. N. K. Dhar, "IR Material Research at the Army Research Laboratory," Invited Keynote Paper, *Proceedings of SPIE*, Vol. 6542, 65420C (2007).
5. Ashok K. Sood, Robert A. Richwine, Yash R. Puri, Nibir K. Dhar, Dennis L. Polla, and Priyalal S. Wijewarnasuriya, "Multispectral EO/IR sensor model for evaluating UV, visible, SWIR, MWIR and LWIR system performance," *Proc. of SPIE* Vol. 7300, 73000H (2009).
6. R. D. Dupuis, H. J. Ryou, D. Yoder et al, "High-performance GaN and AlGaIn ultraviolet avalanche photodiodes grown by MOCVD on bulk III-N substrates," *Proc. of SPIE*, Vol. 6739, 67391B-1-14 (2007).
7. S. C. Shen, Y. Chang, J. B. Limb, J. H. Ryou, P. D. Yoder and R.D. Dupuis, "Performance of Deep UV GaN Avalanche Photodiodes Grown by MOCVD," *IEEE Photonics Technology Letters*, Vol. 19, Number 21, November 2007.
8. Y. Zhang, S. C. Shen, H. J. Kim, S. Choi, J. H. Ryou, R. D. Dupuis and B. Narayan, "Low-Noise GaN Ultraviolet p-i-n photodiodes on GaN Substrates," *Applied Physics Letters*, Vol. 94, 221109 (2009).
9. Ashok K. Sood, Robert A. Richwine, Yash R. Puri, Russell D. Dupuis, Nibir K. Dhar and Raymond S. Balcerak, "Development of GaN/AlGaIn APD's for UV Imaging Applications," *Proceedings of SPIE*, Vol. 7780, 77800E (2010).